Kraft black liquor as a carbonaceous source for the generation of porous monolithic materials and applications toward hydrogen adsorption and ultrastable supercapacitors

Romain Poupart, Ronan Invernizzi, Liliane Guerlou-Demourgues, Jacob Olchowka, Marie Anne Dourges, Jean-Louis Bobet, Hervé Deleuze, Rénal Backov

Kraft Black Liquor as a Carbonaceous Source for the Generation of Porous Monolithic Materials and Applications towards Hydrogen Adsorption and Ultra-stable Supercapacitors

Romain Poupart[1, 2, 3], *Ronan Invernizzi*[2,3], *Liliane Guerlou-Demourgues*[2,4*], *Jacob Olchowka*[2,4], *Marie-Anne Dourges*[1], *Jean-Louis Bobet*[2], *Hervé Deleuze*[1*] *and Rénal Backov*[3]

[1] Univ. Bordeaux, CNRS, Bordeaux INP, ISM, UMR 5255, F-33400 Talence, France

[2] Univ. Bordeaux, CNRS, Bordeaux INP, ICMCB, UMR 5026, F-33600 Pessac, France

[3] Univ. Bordeaux, CNRS, CRPP, UMR 5031, F-33600 Pessac, France

[4] RS2E, Réseau Français sur le Stockage Electrochimique de l'Energie, FR CNRS 3459, France

[*]corresponding author: liliane.guerlou-demourgues@icmcb.cnrs.fr; herve.deleuze@u-bordeaux.fr

Abstract: High internal phase emulsions (HIPEs) have templated self-standing porous carbonaceous materials (carboHIPEs) while employing Kraft Black Liquor, a paper milling industry by-product, as a carbon precursor source. As such, the starting emulsion has been prepared through a laboratory-made homogenizer while native materials have been characterized

at various length scales either with Raman spectrometry, XRD, mercury intrusion porosimetry and nitrogen absorption. After thermal carbonization, specific surface areas ranging from around 600 to 1500 $m^2.g^{-1}$ have been reached while maintaining a monolithic character. Despite a poor graphitization yield, the carbonaceous materials offer a good electronic transport properties reaching 31 $S.m^{-1}$. When tested towards energy storage applications, the native unwashed materials revealed a hydrogen storage of 0.07 wt.% at 40 bar & RT, while hydrogen retention is reaching 0.37 wt.% at 40 bar & RT for the washed sample. When employed as supercapacitor electrodes, these carbonaceous foams are able to deliver high capacities of ~ 140 F/g at 1 A/g, matching thus the ones obtained from a commercial carbon reference, while providing additionally a restored remnant capacity of 120 F/g at 2 A/g over 5,000 cycle numbers.

Keywords: Emulsion templating, Kraft Black Liquor, Carbonaceous foams, Hydrogen storage, Supercapacitors

Introduction

Nowadays, the interest in porous materials has increased significantly among all fields of chemistry, as they are composed either of inorganic, organic or hybrid skeletons.[1] Additionally to their intrinsic chemical nature, these porous materials are reaching a tremendous set of applications ranging from heterogeneous catalysis, environmental remediation, energy storage and conversion, acoustic and thermal insulators and so forth.[2,3] While inorganic foams are mostly silica-based materials[4] or zeolites,[5] the organic ones are polymeric materials.[6] To prepare these materials through a rational design, various processes can be applied to address the desired wall morphologies, pore sizes and monolith macroscopic shapes.[4,6] Particularly, the emulsion templating approach appears a versatile technique favouring interconnected macroporous solid state networks, called either polyHIPEs or Si(HIPE) depending respectively on the organic or inorganic precursors chemical nature. The acronym HIPE stands for "High Internal Phase Emulsion". Since the first patents describing the process by Unilever,[7,8] divers emulsions can be employed: direct oil-in-water emulsions (o/w),[9] reverse water-in-oil emulsions (w/o),[10,11] non-aqueous emulsion[12] or, even, double emulsions.[3,13] Considering the organic networks' chemical nature, the range of materials has been expanded from the first materials consisted of styrene-based materials. Today, organic polyHIPE can be obtained through divers polymers generated from free-radical processes like (meth)acrylated.[14,15] Considering the inorganic HIPE counterparts, the range of emulsion-based materials has also been expanded from fully silica-based materials[16] to the generation of binary-oxide HIPEs systems (labelled MUB as "Materials of the University of Bordeaux) dedicated towards environmental applications.[17,18] If on one hand, when addressing inorganic materials, silica is the most abundant oxide on earth minimizing thereby the costs of native porous oxide ceramics, on the other hand a special effort needs to be

performed when employing organic polymer precursors while reducing fossil-based raw materials. As such, a shift toward more bio-related polyHIPE materials is expected.

In this context, the generation of a porous polyHIPE foams has been proposed while employing a waste of the paper milling industry, Kraft Black Liquor or KBL, being an alkaline aqueous suspension mainly composed of degraded lignin and hemicellulose.[19] Under appropriate thermal treatment, these materials are known to produce carbon-based materials (carboHIPEs), constituted mainly of amorphous carbonaceous backbone associated with randomly dispersed graphitized domains.[20] Porous carbon bearing high degree of graphitization are addressing electronic charge transport properties inducing direct application in energy conversion,[21,22] as well as electrode for supercapacitors.[22] These carboHIPE can address also hydrogen storage where their intrinsic microporosity/small mesoporosity becomes here as the criteria of choice.[23] Over the last few decades, several carbon allotropic forms have been investigated as functional material for supercapacitor or hydrogen storages such as carbon nanotubes,[24,25] or activated carbons.[25,26] Nevertheless, to be industrially implementable, functional carbon-based-materials need of being both abundant and cheap. In this regard, KBL represents a carbonaceous precursor's candidate of choice as being a widely available bio-based raw material addressing an annual production ranging from 500 million tons[27] to 1.3 billion tons per year.[28] For this particular reason, using KBL as a precursor source towards the generation of functional carbonaceous materials is of outmost interest. Recently a carbon arising from KBL decorated with Cu zero-valent nanoparticles (transitional metals carbo-reduction) has been employed towards carbon dioxide electrochemical reduction.[29] Up to now versatile carbo(HIPE) offering simultaneously high surface area and good electronic transport properties was missing because high graphitization promotes undoubtedly low surface area and *vice versa*. A compromise

concerning the thermal treatment was missing still. As such, when considering the generation of bio-related carbo(HIPE), this compromise between high surface area and good electronic properties is proposed inhere. We first investigate the use of a home-made homogenizer device to emulsify a chlorinated hydrophobic phase into the alkaline hydrophilic KBL continuous phase. The resulting polyHIPE has been further investigated by SEM and Mercury Intrusion Porosimetry. Once carbonized, final washed KBL-based carbo(HIPE) leads to a highly porous carbonaceous self-standing material. After characterization at several length scales, the disordered carbonaceous foams revealed interesting specific area of 640 $m^2.g^{-1}$ (1550 $m^2.g^{-1}$ when remnant salts have been washed out). Therefore, the KBL-based carbo(HIPE) has been first tested toward hydrogen storage, reaching 0.37 H_2 wt.% at RT. Aside, the KBL-based carbo(HIPE) is offering an electronic conductivity of 30 $S.m^{-1}$. Thereby its competence as supercapacitor electrodes device has also been tested and compared to the commercially available coconut shells-made Kuraray YP80F carbon. The KBL-based carbonaceous electrodes can deliver the same high capacities of 140 F/g at 1 A/g, while providing additionally ultra-stable returned remnant capacity of 120 F/g at 2A/g after 5,000 cycle numbers.

Materials and methods

Materials

Kraft Black Liquor (with an average residual dry mass of around 45%) has been gifted kindly by Smurfit Kappa Cellulose du Pin (Biganos, France). (±)-Epichlorhydrin (purum, ≥99%), Pluronic® F-108, DCE: 1,2-dichloroethane (ACS reagent, ≥99.0%) and poly(tetrafluoroethylene) (PTFE; powder, >40 μm particle size) have been supplied by Sigma-Aldrich/Merck. Isopropanol (≥98%, technical) and diethyl ether (≥99.7%) have been provided by

VWR. Carbon black (acetylene, 100% compressed) has been purchased from Alfa Aesar. All reagents have been used without further purifications. As previously stated,[30] the as-received Kraft black liquor comes as a viscous black liquid. Its major physico-chemical properties are the followings: dynamic viscosity μ= 7000 mPa s at 23 °C; pH = 14; density ρ = 1.3 g mL^{-1}; dry matter amount ≈ 50 wt.%. Phenol group content and total hydroxyl group content of black liquor were determined according to be 0.5 mmol g^{-1} and 0.8 mmol g^{-1}, respectively.[30]

Preparation of the KBL phase

Preparation can be found elsewhere[19,20,30] and have been slightly optimized here. Briefly, a mixture of KBL (20 g) and Pluronic® F-108 (0.9 g) have been gently mixed (100 rpm) together at room temperature until total dissolution of the non-ionic surfactant. Following this, epichlorhydrin (2.2 g) was added dropwise and mixed for 10 minutes.

Emulsification process, drying and washing

Direct emulsification has been obtained using a laboratory-made homogenizer system composed of two polyethylene syringes (60 mL, internal diameter of 29.2 mm) connected using a small section Nylon tube (ID = 11 mm; OD = 4 mm; length = 15 mm), as seen in Figure 1A. The as-prepared continuous alkaline hydrophilic phase has been inserted into one of the syringe, while the internal phase, 1,2-dichloroethane (15 mL) has been added into the second syringe. The direct emulsion has been obtained by successive back and forth passages through the connecting tubing. The passage rate to generate the emulsion was settled at 10-round trip per minute and the emulsification time was settled at 80 minutes. After emulsification process, the emulsion was removed from the syringes and poured into a PTFE cylindrical mold (diameter of 45 mm, height of 15 mm) pinched between two Teflon plates. The mold has been placed in an

oven (Thermo Scientific Heraeus Vacutherm VT6060) heated at 80°C for 24 h in order to allow epichlorhydrin to react with the lignin and hemicellulose. After crosslinking, the monolith was washed in a Soxhlet apparatus two days with isopropanol and one day with diethyl ether before being dried 2 days at 85 °C under vacuum.

Carbonization step

Approximately 200 mg of the native KBL-based monolith has been carbonized in a tubular alumina oven to obtain carboHIPEs, using a slightly adapted protocol from the literature.[20] Briefly, the sample has been degassed under an Argon flux (0.3 $L.min^{-1}$) for 30 minutes, then, (still under the Ar flux) the temperature has been increased to 900 °C with a faster heating rate of 5 $°C.min^{-1}$ along with shorter plateaus at 300, 600 and 900 °C for 1 h each. Cooldown is governed by the oven inertia. Carbonized samples have been labelled carbo(HIPE).

Hydrogen adsorption methodology

Carbo(HIPE) have been directly used for hydrogen adsorption following a known methodology.[25] Typically, 100 mg of materials have been placed into the sample holder of a manually controlled Sieverts' apparatus. Prior to measurements, the apparatus has been degassed under vacuum for 5; 10 and 20 minutes, with filling with argon in-between. Then the sample have been degassed for 1 h at 300 °C to remove any adsorbed species. Then, the sample is placed back to room temperature (approximately 20 °C, temperature monitored by thermometers in the room and close to the sample holder) and was ready for the H_2 adsorption measurements.

Typically, the desired hydrogen pressure is pre-loaded. Then, the desired pressure is expanded into the sample holder chamber at room temperature. The measured pressure drops,

due to the gas expansion both in the chamber and in the sample. After reaching the thermodynamic equilibrium (*i.e.* no more pressure variations), supplemental 15 minutes are imposed to ensure the thermodynamic equilibrium. In order to evaluate the adsorption on a quantitative manner, the same experiment is performed using the same volume of a non-adsorbing material (here, Fontainebleau sand). After each adsorption, the sample is degassed at room temperature. The experiment is performed for pressure of approximately 10; 20; 30 & 40 bar. High purity hydrogen has been used for this experiment.

Electrochemistry methods

Spared samples from the hydrogenations experiments have been used for electrochemical characterizations. Prior any electrochemical testing carbonized KBL samples have been washed thoroughly in deionized water for 24 hours and then dried in a dryer at 80°C overnight. Those washed samples have been also characterized by nitrogen sorption and XRD. Moreover, electrical resistance measurement have been performed onto the dried sample.

At the same time, an electrode was prepared by mixing in a mortar the (washed) active material with carbon black (Alfa Aesar) and polytetrafluoroethylene (PTFE) in a weight ratio of 80/15/5. Once the mixture becomes self-supported, this latter is manually rolled to decrease its thickness and disks of 16 mm diameter are cut. Then, this electrode was pressed at 5 bars during one minute on a nickel foam. The mass loading of each electrode is fixed at 5 $mg.cm^{-2}$. Electrochemical measurements were carried out at 25°C in a 3-electrode system with reference and counter electrodes being a Hg/HgO electrode (1M NaOH) and a platinum wire respectively. The electrolyte was an alkaline solution of 5M KOH.

Instrumentation

SEM have been performed on a Hitachi TM-1000 apparatus (Hitachi High-Technologies Corp., Tokyo, Japan). Sample has been coated with a thin Pt-metal layer prior to analysis. Photographs were taken at several different magnifications between × 500 and × 10,000. Pieces of polyHIPEs (section of about 0.5 cm^2) were mounted on a carbon tab that ensured electronical conductivity.

Sample's macroporosity have been investigated by Mercury Intrusion Porosimetry (MIP) using an Autopore IV 9500 porosimeter (Micromeritics) with the following parameters: contact angle = 130°, Hg surface tension = 485 $mN \cdot m^{-1}$ and maximum intrusion pressure fixed at 124 MPa. The determination of the pore size distributions porosity features was based on the Washburn equation between the applied pressure and the pore size into which mercury intruded.

Raman spectra were recorded in backscattering geometry using a Labram HR (Horiba Group, France) micro spectrometer equipped with a confocal microscope. The experiments were carried out by exciting the samples at the 514.5 nm (2.41 eV) wavelength of an Ar ion laser. The spectral resolution was equal to 6 cm−1 with a confocal hole aperture of 150 µm and a 600 grooves/mm diffraction grating. The laser was focused on the sample by means of a 50× objective (0.75 numerical aperture). The beam power at the sample was around 200 µW to avoid overheating effects due to laser irradiation. Spectra were recorded with an acquisition time of 60 s and 4 accumulations. We proceeded to hand-made baseline corrections of the spectra by means of the LabSpec 5 software before deconvolutions. Deconvolutions has been performed using either a simple 2-points fits for the 500 – 2000 cm^{-1} (D & G) and a 4-points fit for the 2500 – 3250 cm^{-1}, corresponding to the S1-, S2-, S3- & S4-bands.[31]

Specific surface area was determined by recording nitrogen sorption isotherms (77K) with a 3Flex gas sorption analyser (Micromeritics) after degassing the materials at 250°C under

vacuum. The specific surface areas were calculated using the Brunauer, Emmett, and Teller (BET) method from a limited range of pressure in the adsorption curves.

X-ray diffraction has been performed for the carbon material and was recorded on a Philips PANalytical X'Pert Pro equipped with a copper source ($\lambda_{K\alpha1}$ = 0.1540 nm and $\lambda_{K\alpha2}$ = 0.1544 nm). The powder was recorded for about 2 h on the angular range 10–80 ° (2θ), with a 0.02 ° (2θ) step size and a 2.022 ° (2θ) active width in the detector.

Results and discussions

Materials preparation and characterization

HIPE-based materials have been prepared using a laboratory-made emulsification system, where an example is provided with the Figure 1-A. After drying, a brown cylindrical self-standing sample (Fig. 1-B) has been obtained. Crosslinking occurs by the chemical reaction between the alcohol moieties found in lignin and/or hemicellulose with the chlorine and oxirane functions of epichlorhydrin, creating thus glycerol bridges between oligomers.[30,32]

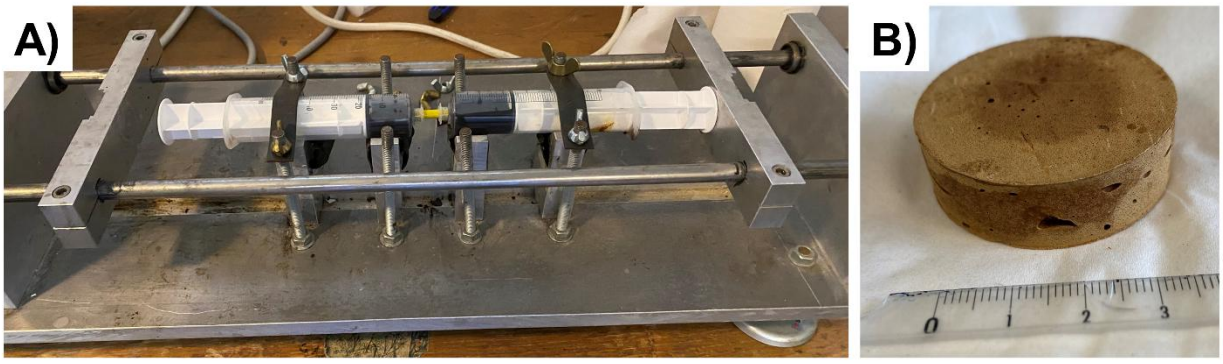

Figure 1: Photography of A) the laboratory-made double-syringe emulsifier in use bearing a KBL/1,2-dichloroethane emulsion and B) a typical KBL poly(HIPE) monolith sample, ruler scale in centimeter.

The morphologies of the brown-greenish polyHIPEs sample have been first characterized at the macroscopic length scale both by SEM and Hg porosimetry. Figure 2-A shows representative pictures of the obtained samples. The materials depict open cellular structures, similar to Poly-(HIPE) foams. The double-syringe process leads to a porous materials bearing typical macroscopic voids characteristic of MIPE-based materials. Moreover, the polydispersity of the macroscopic voids seems to be qualitatively narrow (Fig. 2-C & -E). More quantitatively, the connecting windows between macroscopic cells are well represented through a Gaussian-type distribution, centred on 0.4 µm. (Figure 2-G). Beyond windows diameters distribution, MIP quantified the KBL poly(HIPE) with a 60 % porosity along with an apparent skeletal density of 1.34 $g.mL^{-1}$.

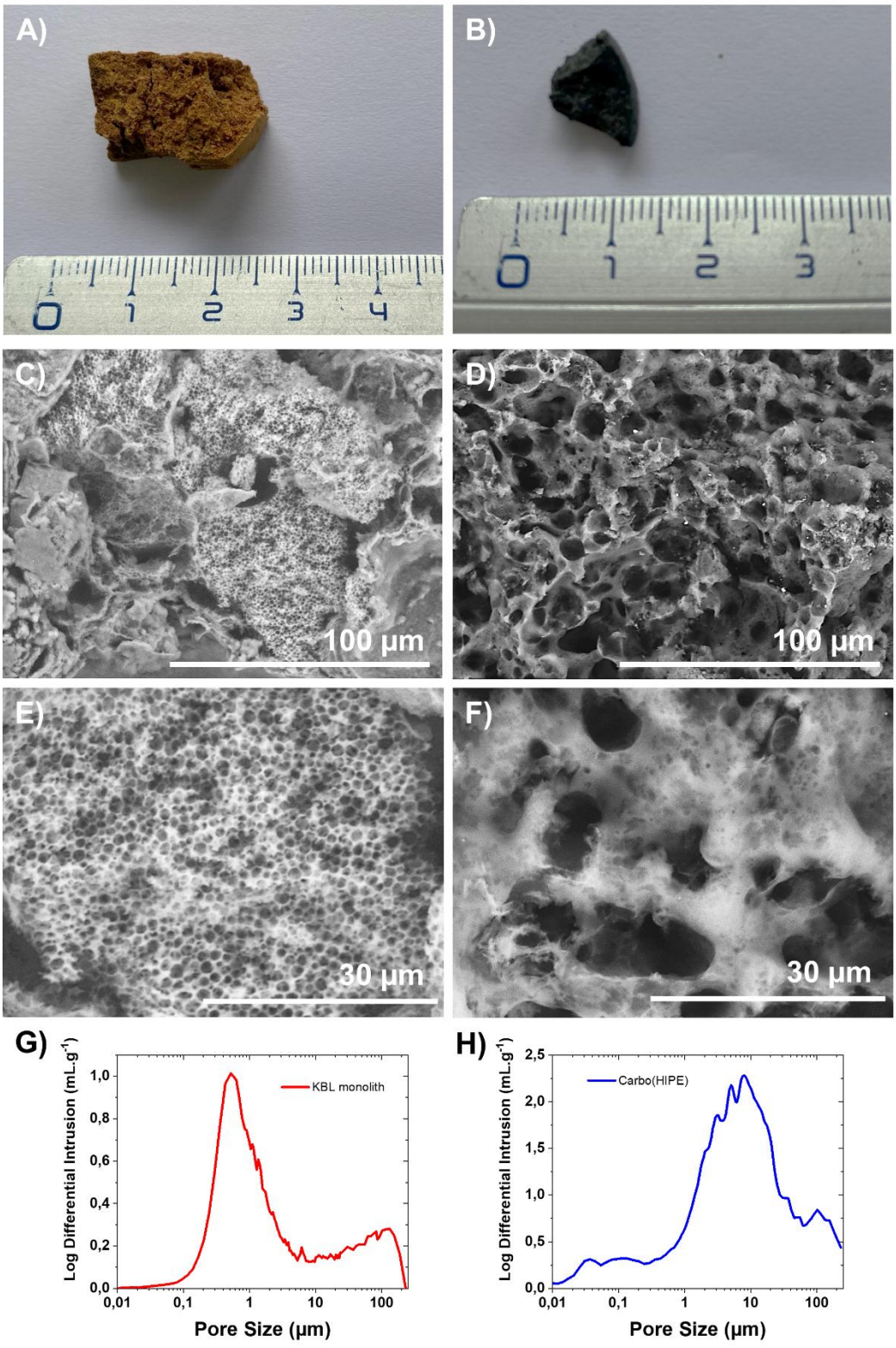

Figure 2: A) & B) Photographs of the samples (ruler in centimeter); C) & D) SEM pictures at lower and E) & F) higher magnification; G) & H) Mercury Intrusion Porosimetry of the KBL and carbo(HIPE) monoliths, respectively. We aim at emphasizing that mercury porosimetry

quantify the geometry that retrained the Hg infiltration this is to say the diameters of cells' connecting windows and not the cell themselves.

Pristine carbonized sample characterization

KBL samples have been carbonized through an updated protocol to generate carbo(HIPE) monoliths (Figure 2-B). Compared to previously reported protocole,[20] the carbonization time scale has been reduced with shorter temperature plateaus (1 h *versus* 4 h at 300 °C & 2 h at 700 and 900 °C, respectively) as well as a higher heating rate (5 °C.min^{-1} *vs*. 1 °C min^{-1}). Diminishing the carbonization time scale promotes overall similar material which can be described still at the microscopic length scale as "disordered carbon", when characterized trough Raman spectroscopy (Fig. 3-A). Indeed, two main bands can be observed in the 1000-1750 cm^{-1} region. First, a band centred at 1337 cm^{-1} that corresponds to disordered sp^2 carbon,[33] so-called D-band. Then, another band centred at 1584 cm^{-1} is observed which corresponds to two dimensional in-plane motion of strongly coupled sp^2 carbons (*i.e.* E_{2g} symmetry) in the honeycomb network of graphite lattice, so-called G-band. The D-band width is larger than the one obtained with the previous, longer protocol (273 cm^{-1} *versus* 225 previously) while the G-band width is smaller (here 106 cm^{-1} *vs.* 125 previously).[20] These differences witness that more microscopic defects are present in this new set of materials while few graphitic domains are remaining still. Concerning the disorder parameter, $I_D/(I_D+I_G)$, with I_D the intensity of the D-band and I_G the intensity of the G-band respectively, appears slightly lower to the one obtained previously (48,9 % here while 50,9 % previously reported), [20] indicating a slightly higher disordered material. Another region in the spectrum to be considered is the 2500-3250 cm^{-1} wavelengths, where the S1-, S2-, S3- & S4-bands (at *c.*2500; 2660; 2900 & 3180 cm^{-1},

respectively) are present.[31] These vibration modes are not well pronounced nor shaped, which corroborates a highly disordered material obtained while enhancing the graphitization kinetic. XRD diffractograms (Figure 3-C) demonstrates the presence of high amount of salts (NaCl, especially but also Na_2CO_3 and Na_2SO_3) within the amorphous carbon materials, as reported in the literature for such carbon precursors.[34] Indeed, these alkaline salts are originally presents in the KBL suspension. In first hand, their presence in the polymeric matrix can enhance the properties of the carbonized materials, as NaCl and sodium carbonate are known to promote graphitization of biomass-based carbon materials during pyrolysis.[35,36] On the other hand , the salt remaining presence can disrupt reaching high specific surface area as addressing intrinsic higher apparent and skeleton densities (specific surface are being expressed in m^2/g) and locking accessibility towards the micro- and mesoscopic voids. Nitrogen adsorption has been performed on this material (Fig. 3-E). A physical artefact during desorption occurred (around $p/p° = 0.5$), due to adsorbed nitrogen condensation within the carbonaceous materials microporosity. Indeed, this artefact is typical of activated carbon,[37] giving the isotherm this specific profile found elsewhere in the literature specifically for carbonaceous materials containing micropores.[20,38] Thereby the observed hysteresis loop between the adsorption and desorption curves cannot be interpreted solely with a presence of mesoporosity. The specific area obtained for such carbonized materials is 640 $m².g^{-1}$, for a volume fraction of the dispersed phase established as 60 %. Compared with similar material, bearing volume fraction of 54 % or 64 %, the present specific area is higher, as obtained surface area were found around 500 $m².g^{-1}$ (respectively 467 and 504 $m².g^{-1}$).[20] Moreover, DFT calculations extrapolated from the nitrogen sorption curves indicate the presence of micropores (*i.e.* pores that does not excess 2.0 nm) or small mesopores (pores between 2.0 and 50 nm) with different peaks below 2 nm (Figure 3-B). The mesopores

offered by the carbo(HIPE) foam are small, falling at the upper limit of the micropores, being contained between 2.0 and 5.0 nm. Carbon materials exhibiting such microporous fixtures are special of interest for different applications, among them, hydrogen storage.[39]

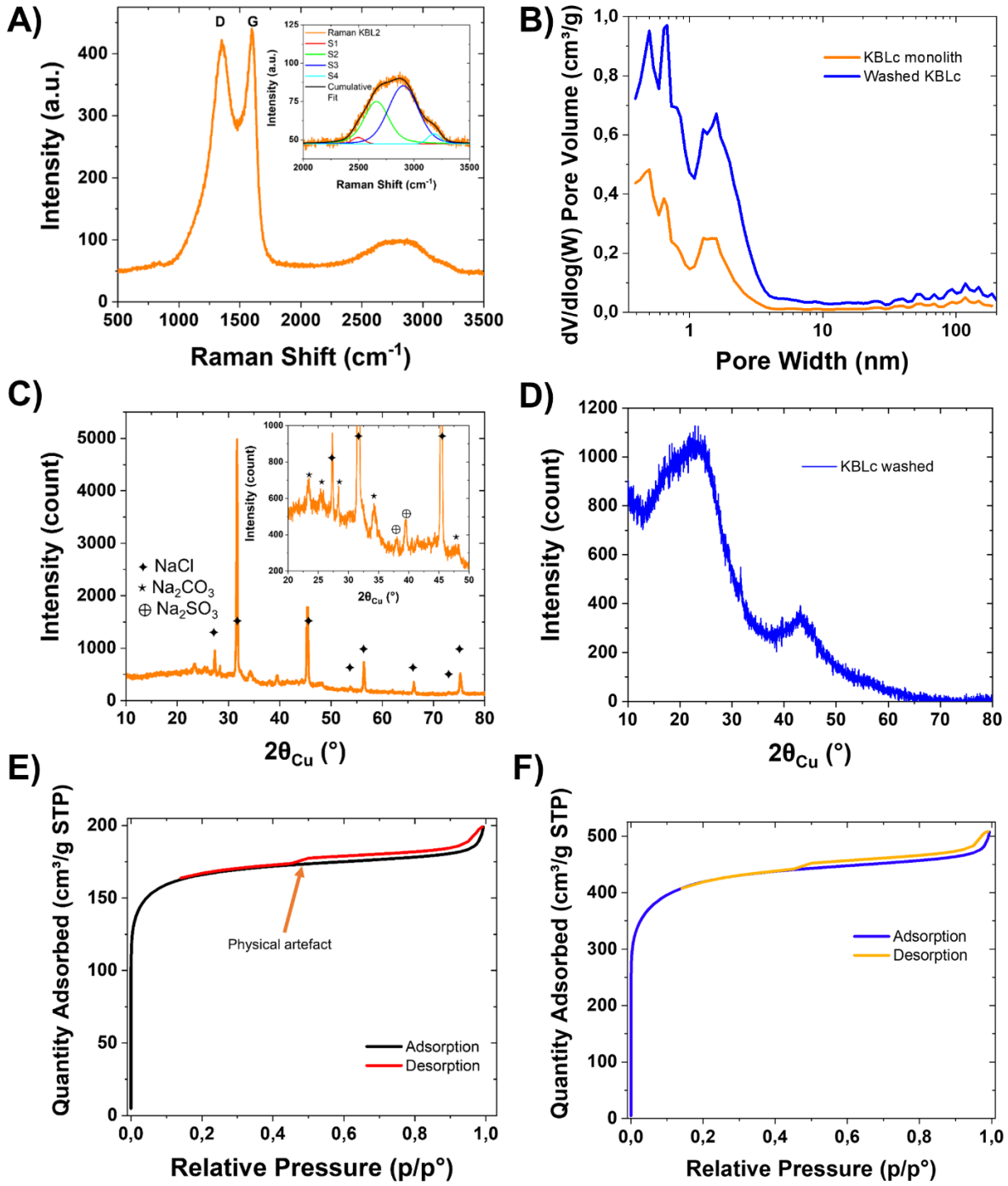

Figure 3: Carbo(HIPE) characterization techniques A) Raman spectroscopy of a carbonized carbo(HIPE) sample (insert: close-up of the 2000-3500 cm^{-1} region); B) respective pore sizes distribution obtained through DFT analysis of the as-carbonized and washed carbo(HIPE) samples; XRD diffractograms of C) the as-carbonized (with ✦ = sodium chloride, ⋆ = sodium carbonate and ⊕ = sodium sulphite highlighted) (insert: close-up of the 20-50 2θ region) & D) of the washed sample, respectively; nitrogen adsorption and desorption profiles of the E) as-carbonized carbo(HIPE) sample & F) of the washed sample, respectively

Washed samples specific characterization

As carbon-based materials arising from biomass are known to be used to prepare carbon-based electrodes for supercapacitors,[40] the KBL-based materials have been tested to such ends. Prior to any electrochemical experiments, the carbo(HIPE)monolith has been washed to remove any salts contained in the matrix, as they can interfere with the analysis (*i.e.* dissolving in the electrolyte during electrochemical tests). However, adding these steps requires newer characterizations, especially for the XRD and nitrogen adsorption. XRD diffractograms (Fig. 3-D) exhibit no traces of the salts anymore, signifying the washing step efficiency, while the weight loss is estimate at 60 wt.%. Two broad diffraction peaks can be observed. The first one at 2θ ranges of 15-25 is attributed to the (002) reflection of graphitic carbon. The weaker diffraction peak at 35-45 (2θ) is attributed to the (101) crystal planes, corresponding to the *a* axis of the graphite structure.[41] Both peaks broadness is indicating the existence of distorted graphite-types units.[42]

The carbonization also keeps the open cellular morphology of the porosity, albeit with larger pores in presence (Fig. 2-D & -F), but still an open porosity. This increase in pore size is confirmed by MIP with the Gaussian type curve centred toward 6 µm (Fig. 2-H). This shift toward higher porosities is mainly attributed to the loss of non-disrupted films between adjacent cells and eventually thinner Plateau borders.[20] Additionally, the carbonization process, reveals a porosity between 10 nm towards 0.1 µm (*i.e.* including mesopores), feature not present before this step. MIP experiments also gives the carbo(HIPE) porosity, with a 71 % value, along with an apparent skeletal density of 0.67 $g.mL^{-1}$.

Considering the nitrogen adsorption, the profile obtained is the same, as shown with Figure 3-F, depicting the physical artefact typical of carbon material presents as well. After analyses, the surface is measured to be 1550 $m^2.g^{-1}$, more than twice of the initial material before washing and making it a strong contender for supercapacitor applications.[43] Again, the DFT calculations allow to determine the pores distribution and reveal once more the presence of micropores (3-B). However, as with the specific area, the washing-step allows an increase in the pores volumes, implying the removal of the salts to gain new spaces. This new pores volume increases the presence of pores below 1 nm.

Hydrogen adsorption of the carbonized material

Following the bio-based carbonized sample preparation, one possible application toward hydrogen adsorption has been investigated. Carbon-based materials are widely known to adsorb hydrogen.[25] Figure 4 demonstrates that at room temperature, the unwashed carbo(HIPE) material exhibit very low adsorption, less than a percent, with a linear profile. This poor adsorption property is not surprising as the critical temperature for adsorption is lower, at 33 K. Upon washing, as the specific area increases, the rate of adsorption increase ever more, with a 4-time higher rate of adsorption, akin to the difference in specific area. Upon doing this washing step, the maximum reached for hydrogen adsorption at 40 bar is up to 0.37 wt.%, better than commercially available NORIT activated carbons that adsorb only 0.25 wt.% at the same pressure.[44]

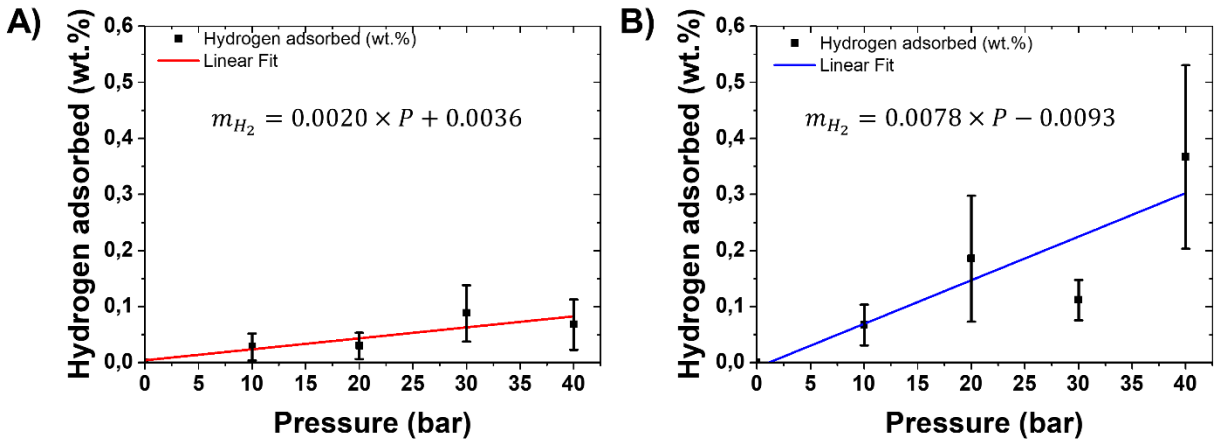

Figure 4: A) Carbo(HIPE) unwashed sample hydrogen adsorption isotherms and. B) carbo(HIPE) washed sample hydrogen adsorption isotherms. Experiments performed at a recorded room temperature (≈ 20 °C).

Electrochemical characterization of the washed samples

At first, conductivity experiments have been performed using a laboratory-made resistivity experimental device. Conductivity is extracted from resistivity (σ= 1/R * L/S) and is evaluated at 30 $S.m^{-1}$. This value is better than carbon xerogels reported in the literature but lower than commercial carbon black, namely Vulcan XC-72R.[45] The carbo(HIPE) monolith electrochemical properties were assessed under cyclic voltammetry and galvanostatic charges/discharges employing 5M KOH aqueous electrolyte. The carbon material voltammogram (Figure 5-A) exhibits a rectangular-like shape suggesting both a good electronic conductivity in the aqueous electrolyte and a capacitive behaviour.[46] Moreover, the galvanostatic charge/discharge curves, illustrated on Figure 5-B, reveal no shape modification when the current density increases from 0.5 A/g to 10 A/g, where the typical triangular signature of capacitive materials remains. Besides, as shown on the figure 5-C, the evolution of the capacitance when the current density increases from 0.5 to 10 A/g (full charge in ~10s), clearly

demonstrates the high capacity retention, addressing a retention value higher than 70% (151 F/g at 0.5 A/g versus 111.2 F/g at 10 A/g). To complete the study, different electrode formulations were also tested and revealed that the carbo(HIPE) alone performs very well at moderate current densities, whereas the addition of carbon black in the electrode formulation (15 wt%) is needed to maintain excellent capacity retention at high current densities (10 A/g) (see Figure S1).

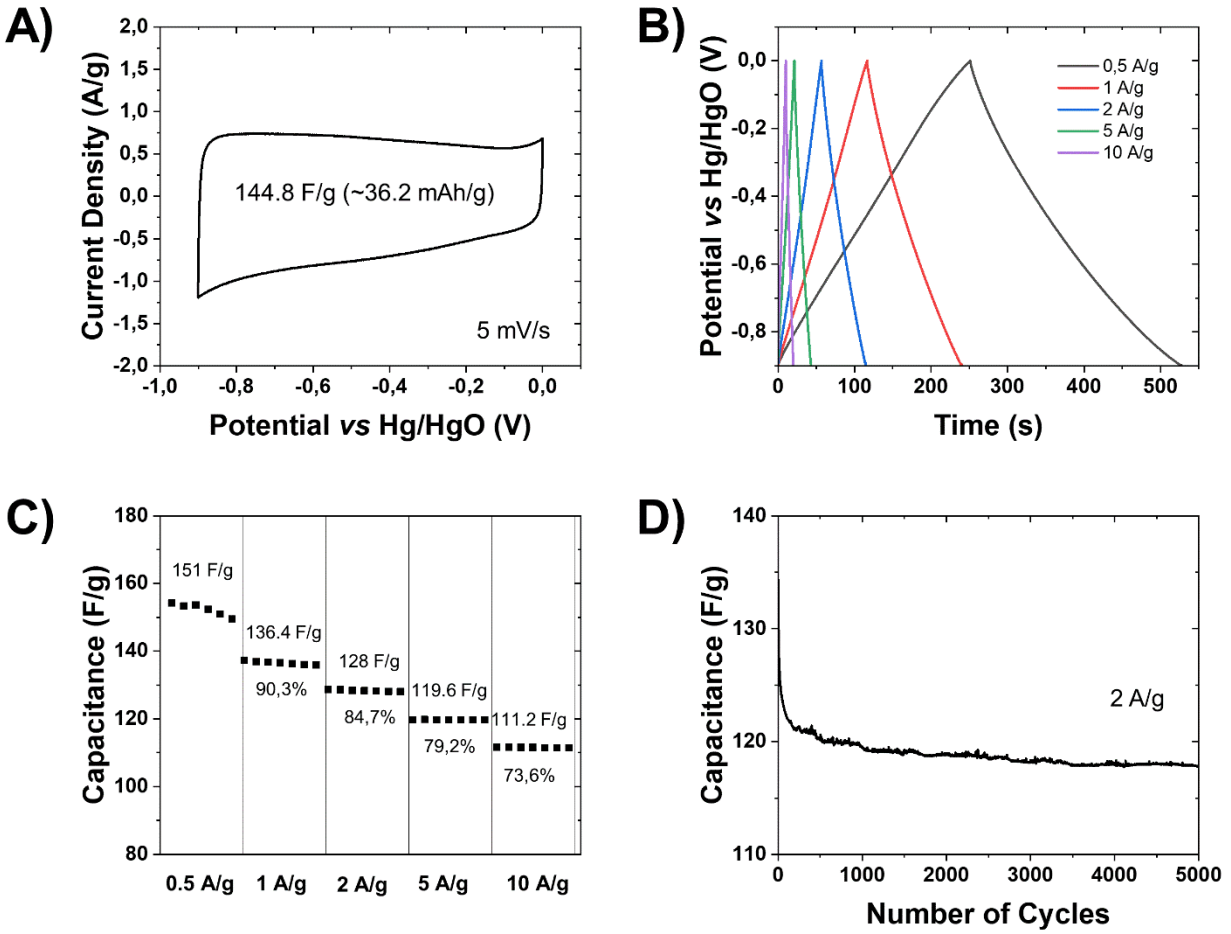

Figure 5: Carbonaceous foams electrochemical investigations. A) Cyclic voltammetry at 5 mV/s in 5M KOH of carboHIPE, B) galvanostatic charge-discharge curves from 0.5 A/g to 10 A/g in 5M KOH, C) Capacity retention at different rate and D) evolution of the capacity at 2 A/g upon long-term cycling.

Finally, except for the first twenty cycles with a capacitance drop of 10 F/g, the capacitance of the carbon material obtained from carbo(HIPE) remains stable over 5000 cycles at 2 A/g, depicting a final capacity of 118 F/g, as illustrated in Fig. 5-D. In comparison, a commercial activated carbon from Kuraray YP80F, which derived from coconut fibers,[47] has been tested in the same conditions, (see Fig. S2) and exhibits similar performance to the carbo(HIPE) electrode in KOH 5M. For instance, at 5 mV/s, the calculated capacitance for YP80F is 164.4 F/g and 144.8 F/g for the carbo(HIPE). These electrochemical results clearly demonstrate that it is possible to employ Kraft black liquor-based carbo(HIPE) electrodes toward electrical double-layer capacitors under outstanding remnant returned capacity while cycling.

Conclusions

A straightforward process is proposed, based on a laboratory-scaled homogenizer, for the preparation of emulsion arising from Kraft black liquor, a waste from the paper industry. This emulsification process can provide monomodal-like distribution of the emulsion's droplets and also allows an easy control of the pore morphology. These polymerized materials have been successfully carbonized through an optimized protocol, being less time consuming. The carbonization provides a rather amorphous carbon material, as described by Raman spectroscopy; containing large amounts of salts, as described by XRD. Nevertheless, this unwashed carbo(HIPE) monolith has been used for H_2 storage, reaching 0.09 wt.% adsorbed at its peak. As carbon arising from biomass-based materials are also currently used in supercapacitor, the carbo(HIPE) sample has been washed to remove residual salts, enhancing the specific area to 1550 $m^2.g^{-1}$, and tested for such purpose. Under the washing treatment, Hydrogen adsorption is increased, reaching 0.37 wt.% at 40 bar. When employed as supercapacitor, its

capacitance reaches 145 F/g at 5 $mV.s^{-1}$ (KOH electrolyte), performance being close to the coconut-based reference material one (Kuraray YP80F). Moreover carbo(HIPE) displays an excellent stability upon long-term cycling. The results obtained with carbo(HIPE) are matching a conventional carbon materials, rendering it an interesting candidate to develop abundant and low cost carbon-based materials to act as energy storage materials for both hydrogen storage and, especially, supercapacitors.

Supporting Information

Specific capacity versus the current density using different electrode formulation and cyclic voltammetry

Author Contributions

The manuscript was written through contributions of all authors. All authors have given approval to the final version of the manuscript. RP generated the sample under the guidance of HD, established the carbonization protocol on his own and performed the hydrogenation experiments under the supervision of JLB. RI performed the electrochemical testing and carbonizations under the supervision of both LGD and JO. MAD performed both nitrogen physisorption measurements and Hg porosimetry while analysing the results in deep. RB supervised and coordinate the whole project.

Acknowledgments

The authors are indebted of the grant "Grands Programmes de Recherche, Post Petroleum Materials –PPM" of the Bordeaux University. The authors thanks Guillaume Clermont, Dr. Nicolas Penin and Anthony Chiron for their helps concerning the thermal treatments, Dr.

Angéline Poulon-Quintin for the helps in the XRD characterizations as well as Pr. Laurent Servant & Dr. David Talaga for the Raman spectroscopy experiments.

References

(1) Brun, N.; Ungureanu, S.; Deleuze, H.; Backov, R. Hybrid Foams, Colloids and beyond: From Design to Applications. *Chem. Soc. Rev.* **2011**, *40* (2), 771–788. https://doi.org/10.1039/B920518G.

(2) Roucher, A.; Depardieu, M.; Pekin, D.; Morvan, M.; Backov, R. Inorganic, Hybridized and Living Macrocellular Foams: "Out of the Box" Heterogeneous Catalysis. *Chem. Rec.* **2018**, *18* (7–8), 776–787. https://doi.org/10.1002/tcr.201700075.

(3) Poupart, R.; Lacour, T.; Darnige, P.; Poncelet, O.; Aristégui, C.; Voisin, T.; Marre, S.; Brunet, T.; Mondain-Monval, O. Elaboration of Soft Porous Ultrasound Insulators. *RSC Adv.* **2020**, *10* (68), 41946–41953. https://doi.org/10.1039/D0RA07269A.

(4) Roucher, A.; Schmitt, V.; Blin, J.-L.; Backov, R. Sol–Gel Process and Complex Fluids: Sculpting Porous Matter at Various Lengths Scales towards the Si(HIPE), Si(PHIPE), and SBA-15-Si(HIPE) Series. *J. Sol-Gel Sci. Technol.* **2019**, *90* (1), 95–104. https://doi.org/10.1007/s10971-018-4794-8.

(5) van Donk, S.; Janssen, A. H.; Bitter, J. H.; de Jong, K. P. Generation, Characterization, and Impact of Mesopores in Zeolite Catalysts. *Catal. Rev.* **2003**, *45* (2), 297–319. https://doi.org/10.1081/CR-120023908.

(6) Wu, D.; Xu, F.; Sun, B.; Fu, R.; He, H.; Matyjaszewski, K. Design and Preparation of Porous Polymers. *Chem. Rev.* **2012**, *112* (7), 3959–4015. https://doi.org/10.1021/cr200440z.

(7) Barby, D.; Haq, Z. Low Density Porous Cross-Linked Polymeric Materials and Their Preparation and Use as Carriers for Included Liquids. US4522953A, June 11, 1985.

(8) Barby, D.; Haq, Z. Low Density Porous Cross-Linked Polymeric Materials and Their Preparation. EP0060138B1, September 3, 1986.

(9) Youssef, C.; Backov, R.; Treguer, M.; Birot, M.; Deleuze, H. Preparation of Remarkably Tough polyHIPE Materials via Polymerization of Oil-in-Water HIPEs Involving 1-Vinyl-5-Aminotetrazole. *J. Polym. Sci., Part A: Polym. Chem.* **2010**, *48* (13), 2942–2947. https://doi.org/10.1002/pola.24075.

(10) Féral-Martin, C.; Birot, M.; Deleuze, H.; Desforges, A.; Backov, R. Integrative Chemistry toward the First Spontaneous Generation of Gold Nanoparticles within Macrocellular polyHIPE Supports (Au@polyHIPE) and Their Application to Eosin Reduction. *React. Funct. Polym.* **10**, *67* (10), 1072–1082. https://doi.org/10.1016/j.reactfunctpolym.2007.06.008.

(11) Desforges, A.; Backov, R.; Deleuze, H.; Mondain-Monval, O. Generation of Palladium Nanoparticles within Macrocellular Polymeric Supports: Application to Heterogeneous Catalysis of the Suzuki–Miyaura Coupling Reaction. *Adv. Funct. Mater.* **2005**, *15* (10), 1689–1695. https://doi.org/10.1002/adfm.200500146.

(12) Kot, E.; Shirshova, N.; Bismarck, A.; Steinke, J. H. G. Non-Aqueous High Internal Phase Emulsion Templates for Synthesis of Macroporous Polymers in Situ Filled with Cyclic Carbonate Electrolytes. *RSC Adv.* **2014**, *4* (22), 11512–11519. https://doi.org/10.1039/C4RA00118D.

(13) Vilanova, N.; Kolen'ko, Y. V.; Solans, C.; Rodríguez-Abreu, C. Multiple Emulsions as Soft Templates for the Synthesis of Multifunctional Silicone Porous Particles. *J. Colloid Interface Sci.* **2015**, *437*, 235–243.

(14) Krajnc, P.; Štefanec, D.; Brown, J. F.; Cameron, N. R. Aryl Acrylate Based High-Internal-Phase Emulsions as Precursors for Reactive Monolithic Polymer Supports. *J. Polym. Sci., Part A: Polym. Chem.* **2005**, *43* (2), 296–303. https://doi.org/10.1002/pola.20501.
(15) Paljevac, M.; Jeřabek, K.; Krajnc, P. Crosslinked Poly(2-Hydroxyethyl Methacrylate) by Emulsion Templating: Influence of Crosslinker on Microcellular Structure. *J. Polym. Environ.* **2012**, *20* (4), 1095–1102. https://doi.org/10.1007/s10924-012-0524-4.
(16) Carn, F.; Colin, A.; Achard, M.-F.; Deleuze, H.; Sellier, E.; Birot, M.; Backov, R. Inorganic Monoliths Hierarchically Textured via Concentrated Direct Emulsion and Micellar Templates. *J. Mater. Chem.* **2004**, *14* (9), 1370–1376. https://doi.org/10.1039/B400984C.
(17) Ly, I.; Vardon, A.; Chanut, N.; Nallet, F.; Pellenq, R. J.-M.; Rouzières, M.; Clérac, R.; Akil, J.; Epron, F.; Especel, C.; Backov, R. Binary CoOx–SiO2 Porous Nanostructures for Catalytic CO Oxidation. *ACS Appl. Nano Mater.* **2022**, *5* (5), 7331–7343. https://doi.org/10.1021/acsanm.2c01258.
(18) Ly, I.; Layan, E.; Picheau, E.; Chanut, N.; Nallet, F.; Bentaleb, A.; Dourges, M.-A.; Pellenq, R. J.; Hillard, E. A.; Toupance, T.; Dole, F.; Louërat, F.; Backov, R. Design of Binary Nb2O5–SiO2 Self-Standing Monoliths Bearing Hierarchical Porosity and Their Efficient Friedel–Crafts Alkylation/Acylation Catalytic Properties. *ACS Appl. Mater. Interfaces* **2022**, *14* (11), 13305–13316. https://doi.org/10.1021/acsami.1c24554.
(19) Foulet, A.; Birot, M.; Sonnemann, G.; Deleuze, H. The Potential of Kraft Black Liquor to Produce Bio-Based Emulsion-Templated Porous Materials. *React. Funct. Polym.* **2015**, *90*, 15–20. https://doi.org/10.1016/j.reactfunctpolym.2015.03.006.
(20) Foulet, A.; Birot, M.; Backov, R.; Sonnemann, G.; Deleuze, H. Preparation of Hierarchical Porous Carbonaceous Foams from Kraft Black Liquor. *Mater. Today Commun.* **2016**, *7*, 108–116. https://doi.org/10.1016/j.mtcomm.2016.04.005.
(21) Kovačič, S.; Schafzahl, B.; Matsko, N. B.; Gruber, K.; Schmuck, M.; Koller, S.; Freunberger, S. A.; Slugovc, C. Carbon Foams via Ring-Opening Metathesis Polymerization of Emulsion Templates: A Facile Method to Make Carbon Current Collectors for Battery Applications. *ACS Appl. Energy Mater.* **2022**. https://doi.org/10.1021/acsaem.2c02787.
(22) Brun, N.; Prabaharan, S. R. S.; Morcrette, M.; Sanchez, C.; Pécastaings, G.; Derré, A.; Soum, A.; Deleuze, H.; Birot, M.; Backov, R. Hard Macrocellular Silica Si(HIPE) Foams Templating Micro/Macroporous Carbonaceous Monoliths: Applications as Lithium Ion Battery Negative Electrodes and Electrochemical Capacitors. *Adv. Funct. Mater.* **2009**, *19* (19), 3136–3145. https://doi.org/10.1002/adfm.200900749.
(23) Xia, Y.; Yang, Z.; Zhu, Y. Porous Carbon-Based Materials for Hydrogen Storage: Advancement and Challenges. *J. Mater. Chem. A* **2013**, *1* (33), 9365–9381. https://doi.org/10.1039/C3TA10583K.
(24) Frackowiak, E.; Delpeux, S.; Jurewicz, K.; Szostak, K.; Cazorla-Amoros, D.; Béguin, F. Enhanced Capacitance of Carbon Nanotubes through Chemical Activation. *Chem. Phys. Lett.* **2002**, *361* (1), 35–41. https://doi.org/10.1016/S0009-2614(02)00684-X.
(25) Panella, B.; Hirscher, M.; Roth, S. Hydrogen Adsorption in Different Carbon Nanostructures. *Carbon* **2005**, *43* (10), 2209–2214. https://doi.org/10.1016/j.carbon.2005.03.037.
(26) Hulicova-Jurcakova, D.; Seredych, M.; Lu, G. Q.; Bandosz, T. J. Combined Effect of Nitrogen- and Oxygen-Containing Functional Groups of Microporous Activated Carbon

on Its Electrochemical Performance in Supercapacitors. *Adv. Funct. Mater.* **2009**, *19* (3), 438–447. https://doi.org/10.1002/adfm.200801236.

(27) Kevlich, N. S.; Shofner, M. L.; Nair, S. Membranes for Kraft Black Liquor Concentration and Chemical Recovery: Current Progress, Challenges, and Opportunities. *Sep. Sci. Technol.* **2017**, *52* (6), 1070–1094. https://doi.org/10.1080/01496395.2017.1279180.

(28) Pola, L.; Collado, S.; Oulego, P.; Díaz, M. Kraft Black Liquor as a Renewable Source of Value-Added Chemicals. *Chem. Eng. J.* **2022**, *448*, 137728. https://doi.org/10.1016/j.cej.2022.137728.

(29) Fonseca, B. C. da S.; Araújo, L. S.; Pinheiro, B. da S.; Santos, A. S. dos; Amaral-Labat, G.; Matsushima, J. T.; Baldan, M. R. Bio-Based Carbon Electrochemically Decorated with Cu Nanoparticles: Green Synthesis and Electrochemical Performance. *Mater. Res.* **2022**, *25*.

(30) Forgacz, C.; Birot, M.; Deleuze, H. Synthesis of Porous Emulsion-Templated Monoliths from a Pulp Mill by-Product. *J. Appl. Polym. Sci.* **2013**, *129* (5), 2606–2613. https://doi.org/10.1002/app.38981.

(31) Henry, D. G.; Jarvis, I.; Gillmore, G.; Stephenson, M. Raman Spectroscopy as a Tool to Determine the Thermal Maturity of Organic Matter: Application to Sedimentary, Metamorphic and Structural Geology. *Earth Sci. Rev.* **2019**, *198*, 102936. https://doi.org/10.1016/j.earscirev.2019.102936.

(32) Forgacz, C.; Birot, M.; Deleuze, H. Synthesis of Macroporous Monolithic Materials from a Waste Renewable Source. *J. Appl. Polym. Sci.* **2015**, *132* (1). https://doi.org/10.1002/app.41215.

(33) Merlen, A.; Buijnsters, J. G.; Pardanaud, C. A Guide to and Review of the Use of Multiwavelength Raman Spectroscopy for Characterizing Defective Aromatic Carbon Solids: From Graphene to Amorphous Carbons. *Coatings* **2017**, *7* (10). https://doi.org/10.3390/coatings7100153.

(34) Foulet, A. Application de l'analyse du cycle de vie lors de la conception de matériaux poreux à partir de la biomasse. Thesis, Université de Bordeaux, 2015. https://tel.archives-ouvertes.fr/tel-01325242.

(35) Shi, R.; Han, C.; Li, H.; Xu, L.; Zhang, T.; Li, J.; Lin, Z.; Wong, C.-P.; Kang, F.; Li, B. NaCl-Templated Synthesis of Hierarchical Porous Carbon with Extremely Large Specific Surface Area and Improved Graphitization Degree for High Energy Density Lithium Ion Capacitors. *J. Mater. Chem. A* **2018**, *6* (35), 17057–17066. https://doi.org/10.1039/C8TA05853A.

(36) Jalalabadi, T.; Moghtaderi, B.; Allen, J. The Interplay between Ternary Molten Carbonate and Biomaterials during Pressurized Slow Pyrolysis. *React. Chem. Eng.* **2022**, *7* (3), 674–690. https://doi.org/10.1039/D1RE00544H.

(37) Lai, W.; Yang, S.; Jiang, Y.; Zhao, F.; Li, Z.; Zaman, B.; Fayaz, M.; Li, X.; Chen, Y. Artefact Peaks of Pore Size Distributions Caused by Unclosed Sorption Isotherm and Tensile Strength Effect. *Adsorption* **2020**, *26* (4), 633–644. https://doi.org/10.1007/s10450-020-00228-1.

(38) Fomkin, A. A.; Dubovik, B. A.; Limonov, N. V.; Pribylov, A. A.; Pulin, A. L.; Men'shchikov, I. E.; Shkolin, A. V. Methane Adsorption on Microporous Carbon Adsorbent Prepared from Thermochemically Activated Wood. *Prot. Met. Phys. Chem. Surf.* **2021**, *57* (1), 17–21. https://doi.org/10.1134/S2070205121010081.

(39) Choi, Y.-K.; Park, S.-J. Preparation and Characterization of Sucrose-Based Microporous Carbons for Increasing Hydrogen Storage. *J. Ind. Eng. Chem.* **2015**, *28*, 32–36. https://doi.org/10.1016/j.jiec.2015.02.012.

(40) Keppetipola, N. M.; Olivier, C.; Toupance, T.; Cojocaru, L. Biomass-Derived Carbon Electrodes for Supercapacitors and Hybrid Solar Cells: Towards Sustainable Photo-Supercapacitors. *Sustainable Energy Fuels* **2021**, *5* (19), 4784–4806. https://doi.org/10.1039/D1SE00954K.

(41) Liu, X.-Y.; Huang, M.; Ma, H.-L.; Zhang, Z.-Q.; Gao, J.-M.; Zhu, Y.-L.; Han, X.-J.; Guo, X.-Y. Preparation of a Carbon-Based Solid Acid Catalyst by Sulfonating Activated Carbon in a Chemical Reduction Process. *Molecules* **2010**, *15* (10), 7188–7196. https://doi.org/10.3390/molecules15107188.

(42) Le, H. T. T.; Dang, T.-D.; Chu, N. T. H.; Park, C.-J. Synthesis of Nitrogen-Doped Ordered Mesoporous Carbon with Enhanced Lithium Storage Performance from Natural Kaolin Clay. *Electrochimica Acta* **2020**, *332*, 135399. https://doi.org/10.1016/j.electacta.2019.135399.

(43) Keppetipola, N. M.; Dissanayake, M.; Dissanayake, P.; Karunarathne, B.; Dourges, M. A.; Talaga, D.; Servant, L.; Olivier, C.; Toupance, T.; Uchida, S.; Tennakone, K.; Kumara, G. R. A.; Cojocaru, L. Graphite-Type Activated Carbon from Coconut Shell: A Natural Source for Eco-Friendly Non-Volatile Storage Devices. *RSC Adv.* **2021**, *11* (5), 2854–2865. https://doi.org/10.1039/D0RA09182K.

(44) Ströbel, R.; Jörissen, L.; Schliermann, T.; Trapp, V.; Schütz, W.; Bohmhammel, K.; Wolf, G.; Garche, J. Hydrogen Adsorption on Carbon Materials. *Journal of Power Sources* **1999**, *84* (2), 221–224. https://doi.org/10.1016/S0378-7753(99)00320-1.

(45) Alegre, C.; Sebastián, D.; Baquedano, E.; Gálvez, M. E.; Moliner, R.; Lázaro, M. J. Tailoring Synthesis Conditions of Carbon Xerogels towards Their Utilization as Pt-Catalyst Supports for Oxygen Reduction Reaction (ORR). *Catalysts* **2012**, *2* (4), 466–489. https://doi.org/10.3390/catal2040466.

(46) Gu, W.; Yushin, G. Review of Nanostructured Carbon Materials for Electrochemical Capacitor Applications: Advantages and Limitations of Activated Carbon, Carbide-Derived Carbon, Zeolite-Templated Carbon, Carbon Aerogels, Carbon Nanotubes, Onion-like Carbon, and Graphene. *WIREs Energy Environ.* **2014**, *3* (5), 424–473. https://doi.org/10.1002/wene.102.

(47) Kostoglou, N.; Koczwara, C.; Stock, S.; Tampaxis, C.; Charalambopoulou, G.; Steriotis, T.; Paris, O.; Rebholz, C.; Mitterer, C. Nanoporous Polymer-Derived Activated Carbon for Hydrogen Adsorption and Electrochemical Energy Storage. *Chem. Eng. J.* **2022**, *427*, 131730. https://doi.org/10.1016/j.cej.2021.131730.

Table of Content